Supramolecular Assembly of Polyphenols and Nucleic Acids by Thermal Cycling for Immune Cell Activation

Yijiao Qu[a,‡], Haiyan Zhu[b,‡], Zhixing Lin[a], Domitilla Vanni[a,c], Sukhvir Kaur Bhangu[b], Brendan Dyett[b], Marc-Antoine Sani[d], Christina Cortez-Jugo[a], Frank Caruso[a]* and Francesca Cavalieri[b, c]*

[a]Department of Chemical Engineering, The University of Melbourne, Parkville, Victoria 3010, Australia

[b]School of Science, RMIT University, Melbourne, Victoria 3000, Australia

[c]Dipartimento di Scienze e Tecnologie Chimiche, Universita' di Roma "Tor Vergata,"

Via della Ricerca Scientifica 1, Rome 00133, Italy

[d]The Bio21 Institute, The University of Melbourne

Melbourne, Victoria 3010, Australia

ABSTRACT: Supramolecular assembly of polyphenols and biomacromolecules (proteins and nucleic acids) has emerged as a versatile and simple strategy to construct nanomaterials with biological activity. Here, we report a strategy to finely control the supramolecular assembly of tannic acid and oligonucleotides into uniform and stable nanoparticles by exploiting the thermal cycling of tannic acid. The equilibrium of complexation is investigated, and individual nanoparticles are resolved with nanoscale resolution using stochastic optical reconstruction microscopy. The nanoparticles incorporating cytosine phosphoguanine (CpG) oligonucleotides are efficiently taken up by cells and trafficked via endo/lysosomal compartments and induce up to a 7-fold increase in tumor necrosis factor secretion in RAW 264.7 macrophage cells compared with naked CpG oligonucleotides. This work highlights the potential of this simple approach to engineer two-component tannic acid–oligonucleotide nanoparticles for the intracellular delivery of therapeutic nucleic acids.

Introduction

Particle-mediated intracellular delivery of exogenous and precisely engineered nucleic acids is a promising method for treating various chronic diseases, infections, and cancers.[1-4] Microparticles have been engineered to serve as nucleic acid delivery systems; however, nanoparticles (NPs) are generally considered ideal systems for in vivo delivery of nucleic acids owing to their prolonged circulation half-life.[5,6] Inorganic nanoparticles (gold, silica, iron oxide and lanthanides) provide platforms for delivery of nucleic acids via pore and gate keeper encapsulation, chemical conjugation and physical surface adsorption[7]. However nucleic acid delivery systems are primarily prepared via the complexation of DNA or RNA molecules with positively charged and ionizable lipids, polymers, via electrostatic interactions.[6,8] The complexation between nucleic acids and lipids or polymers is essential to avoid the enzymatic degradation of nucleic acids by nucleases

2

and enable their internalization and intracellular trafficking in the target cells. However, owing to their nonspecific electrostatic and hydrophobic interactions with cell membranes, synthetic cationic or ionizable lipids and polymers have also shown undesirable adverse and off-target effects, such as toxicity and enhanced undesired immune responses in vitro and in vivo.[9] Supramolecular assembly of nucleic acids with natural, degradable, and noncationic biomolecules via strong hydrogen bonds and hydrophobic interactions may provide an alternative strategy for engineering less toxic and efficient nucleic acid delivery vehicles. Tannic acid (TA) belongs to the category of plant/derived polyphenols and has attracted growing interest in biomaterial science, as it is generally recognized as safe by the US Food and Drug Administration.[10] TA has a multibranched molecular structure containing ten gallol and catechol groups that can interact with various metal ions, and synthetic and natural polymers via diverse intermolecular interactions.[11-15] The supramolecular assembly of TA with polymers is typically regulated by hydrogen bonding and electrostatic interactions.[11-15] For example, the strong hydrogen bonding between polyphenols, poly(ethylene glycol) (PEG), and poly(N-vinylpyrrolidone) allows the formation of nanocomplexes that have shown potential in the oral delivery of antibodies[16] and anticancer drugs[17] and nasal delivery of vitamin E[18]. A one-pot assembly of biomacromolecules (proteins and siRNA), metal ions, polyphenols, and PEG was recently reported to construct bioactive NPs stabilized by metal–phenolic coordination and hydrophobic interactions.[19] Template-mediated assembly of proteins and polyphenols (e.g., TA) on various substrates (e.g., organic, inorganic, and biological entities) enabled the formation of protein–polyphenol network microparticles without requiring the addition of metals or synthetic polymers.[20] The template-mediated assembly of TA and DNA was likewise recently exploited to fabricate microparticles solely made of DNA

and TA, with different morphologies stabilized by both hydrogen bonding and π–π stacking interactions.[21]

Despite efforts to fabricate polyphenol-based nano- and microparticles by supramolecular assembly, the synthesis of these systems relies on the use of templates, redox-active metal ions, and/or nondegradable synthetic polymers (e.g., PEG) to promote complexation and stabilization of the NPs.[22,23] Ha et al.[24] reported the preparation of TA–DNA nanocomplexes via assembly for gene release in cancer cells; however, because of the uncontrolled assembly of the two molecules, polydisperse aggregates were obtained, which are unsuitable for in vivo administration. Therefore, there is a need for alternative methods to prepare polyphenol–DNA NPs in a controlled fashion by leveraging template-, metal-, and synthetic polymer-free supramolecular assembly processes.

Herein, we introduce a simple and facile approach to finely control the supramolecular assembly of TA and oligonucleotides (ODN) into uniform and stable NPs in the absence of templates, metal ions, and nondegradable synthetic polymers. The kinetics of the supramolecular assembly process and the molecular arrangement of the two building blocks, i.e., TA and ODNs, was controlled by a heating–cooling process. The structure and morphology of the NPs were investigated by stochastic optical reconstruction microscopy (STORM). This imaging method also allowed evaluation of the equilibrium of complexation and nanoscale resolution of individual NPs based on the detection of single-molecule localizations. ODNs containing immunostimulatory unmethylated cytosine–guanine (CpG) motifs were used for immune cell activation. STORM enabled probing the endosomal escape of the TA–ODN NPs. Moreover, the obtained NPs showed limited cytotoxicity against macrophage cells, were efficiently taken up by cells, trafficked via endo/lysosomal compartments, and induced an immunostimulatory effect in macrophages. Collectively, this work highlights the heat-induced supramolecular complexation of TA and DNA

as an alternative approach to preparing self-assembled NPs for the effective loading and delivery of therapeutic ODNs.

Experimental Section

Materials: The CpG-containing ODN used in this study, TGCAAGCTGTTGAGTCGACGTTAAGAGCCTGCTGAAGCGTCTGCGA (47mer), was synthesized and purified by Sangon Biotech Co., Ltd. (Shanghai, China). HPLC-purified ODNs sequences……..(15 mer) and ….(60 mer) were purchased from Biosearch Technologies (Risskov, Denmark). TA, (3-(4,5-dimethylthiazol-2-yl)-2,5-diphenyltetrazolium bromide (MTT), dimethyl sulfoxide (DMSO), phosphate-buffered saline (PBS), Dulbecco's phosphate-buffered saline (DPBS), and FBS were purchased from Sigma-Aldrich (St. Louis, MO, USA). Trihydrochloride (Hoechst 33342), Dulbecco's modified Eagle's medium (DMEM), Alexa Fluor 488–wheat germ agglutinin conjugate (AF488–WGA), LysoTracker Green, and trypsin were obtained from Life Technologies. Rabbit anti-Rab7, rabbit anti-EEA1, and monoclonal antibodies were purchased from Cell Signaling Technology (Danvers, MA, USA). Mouse anti-LAMP-1 antibody and Alexa Fluor secondary conjugates were supplied by Invitrogen (Carlsbad, CA, USA). Enzyme-linked immunosorbent assay (ELISA) kit of TNF-α was purchased from Invitrogen. Rabbit-EEA-1 monoclonal antibody, rabbit-Rab7 monoclonal antibody, rabbit LAMP-1 and goat anti-rabbit conjugate secondary antibody were purchased from Cell Signalling Technology. All chemicals were used as received without further purification. Ultrapure water with a resistivity of greater than 18 MΩ cm was used in all experiments and obtained from a three-stage Millipore Milli-Q Plus 185 purification system.

Preparation of TA–ODN NPs: The TA–ODN NPs were synthesized via a facile one-pot self-assembly method. An aqueous solution of TA (40 µL, 5 mg mL^{-1}) was added to an aqueous solution of ODN (60 µL, 38 µM). The mixture was incubated at 90 °C for 1 h and cooled to 20 °C at ~0.5 °C s^{-1}. The resulting TA–ODN NPs were retrieved by centrifugation at 10000 g for 15 min. To probe the effect of the TA/ODN weight ratio, the amount of TA was increased while the amount of ODN was fixed.

Characterization of TA and TA–ODN NPs: ^{1}H NMR spectra were recorded on an Agilent MR400 and acquired using the following parameters: 16 scans, 3 s relaxation delay, and spectral width of 9.6 kHz. The spectra were processed using MestreNova 14.2.3 and ^{1}H chemical shifts were referenced to trimethylsilylpropanoate-d$_4$ at 0 ppm. The stability of TA was assessed by first dissolving TA in water, followed by heating on a ThermoMixer for 1 h at 95 °C, and subsequently subjected to HPLC analysis on a high-performance liquid chromatography system (1260 Infinity II, Agilent Technology Company, USA) equipped with a 5 µm C18 column (RESTEK, 150 mm × 4.6 mm). For comparison purposes, untreated TA was also analyzed. For HPLC analysis, the samples (20 µL, 500 µg mL^{-1}) were filtered through a 0.22 µm filter membrane and injected using acetonitrile as the gradient eluent. A binary mobile phase containing eluent A, 0.1% trifluoroacetic acid in water, and eluent B, acetonitrile, was used. The gradient elution program was as follows: 0–30 min, 10–70% eluent B; 30–30.01 min, 70–10% eluent B; and 30.01–41 min, 10% eluent B. The ζ-potential and size distribution of the particles were measured on a Zetasizer Nano-ZS instrument (Malvern Instruments, UK). TEM analysis was conducted at an operation voltage of 120 kV. Prior to TEM imaging, the samples (5 µL) were deposited on formvar carbon-coated copper grids, which were precleaned using plasma. For AFM imaging, a sample solution (10 µL)

was deposited onto a clean glass substrate overnight and imaged in tapping mode. For SEM imaging, dried samples were sputter-coated with gold prior to imaging.

For STORM analysis, AF647-labeled TA–ODN NPs were prepared as described above using different TA/ODN weight ratios of 1:1, 4:1, 7:1, 10:1, and 12:1. To obtain an optimal signal density for STORM imaging, only one-fourth of the required DNA strands were used in the labeled form for the preparation of the TA–ODN NPs. For serum stability studies AF647-labeled TA–ODN NPs were mixed with different concentrations of Fetal Bovine Serum, FBS, (10 and 100 %) for 3 h. The obtained AF647-labeled TA–ODN NPs were then deposited on a glass slide. After deposition for 30 min at 25 °C, unbound molecules and NPs were washed away with freshly prepared, standard imaging buffer with cysteamine. STORM images were acquired using a Nikon N-STORM system equipped with a Nikon 100× 1.4 NA oil immersion objective. The focus and the total internal reflection fluorescence imaging angle were adjusted to obtain a high signal-to-noise ratio. The 647 nm laser was used for the excitation of the fluorophores. All time lapses were recorded within a 256 pixels × 256 pixels region using an EMCCD camera. For each image, 4000 frames were acquired sequentially using full laser power. STORM images were first processed with the STORM module of the NIS Elements Nikon software, where drift correction was performed, and a list of particle localizations were obtained by Gaussian fitting of the fluorescence spots of blinking dyes. Blinking events that were detected in ≤5 consecutive frames were counted as single molecules, whereas events detected in more than 5 consecutive frames were discarded (maximum trace length 5). The list of localizations was exported as a .txt file and analyzed using a clustering analysis script in Python, where the localizations were clustered using a kernel density estimation with a bandwidth of 50 nm. An ellipse was fitted to the obtained clusters with a minimum of 10 localizations and a maximum elongation factor of 1.5 (ratio of long and short axes

of the ellipse). Then, the circles containing 90% of detected spots in the cluster were fitted to determine the size distribution of the NPs and the number of localizations.

Cell Cultures: RAW 264.7 cells with a passage number of 36–42 were cultured in complete DMEM supplied with 10% FBS at 37 °C, 5% CO_2, and 95% humidity.

MTT Assays: To measure particle toxicity/cell viability, RAW 264.7 cells were plated in a 96-well culture plate at a density of 1×10^4 cells per well at 37 °C, overnight. Then, cells were incubated with the TA–ODN NPs at different DNA concentrations for 24 h. The culture medium was removed and MTT solution (150 µL, 0.5 mg mL^{-1}) was added to each well and incubated at 37 °C for 4 h. Then, DMSO (50 µL) was added to dissolve formazan. A microplate reader was used to measure the absorbance of the supernatant at 570 nm.

Cell Association: RAW 264.7 cells were plated in a 24-well culture plate at a density of 5×10^4 cells per well overnight. Cells were incubated with TA–ODN NPs prepared with AF488-labeled DNA (DNA: 100 nM) in fresh medium for 2, 4, 8, and 24 h. Then, cells were harvested by trypsinization and washed 3 times with PBS at 400 g for 5 min. The cells were resuspended in DPBS and at least 1×10^4 cells were analyzed by flow cytometry.

Cell Internalization: RAW 264.7 cells were plated in Labtek 8-well chamber slides at a density of 3×10^4 cells per well and incubated overnight. AF647-labeled TA–ODN NPs were added to the cells and incubated for 2, 4, 8, and 24 h at 37 °C, before washing with PBS three times and then fixing the cells with 4% paraformaldehyde for 15 min. The membrane was stained with AF488–WGA (5 µg mL^{-1}) for 5 min and the nucleus was stained with Hoechst 33342 (1 µg mL^{-1}) for 10 min. Finally, cells were imaged with a confocal microscope using a 100× objective (Nikon A1R, Nikon, Japan).

Intracellular Trafficking Evaluated by STORM: For STORM analysis, TA–ODN NPs were dual-labeled using a mixture of AF488- and AF647-labeled DNA during preparation. RAW 264.7 cells were plated at 3×10^4 cells per well in Labtek 8-well chamber slides and incubated overnight. The cells were exposed to dual-labeled AF647/AF488 TA–ODN NPs for 4–28 h. For intracellular trafficking studies, the noninternalized particles were washed out after 4 h incubation and kept at 37 °C for further 0, 4, or 24 h in fresh media. At each timepoint, the cells were fixed with 4% paraformaldehyde for 15 min, washed, permeabilized with 0.1% Triton X-100 solution in PBS for 5 min, and washed again three times with 1% BSA in PBS. The cells were then incubated with rabbit-EEA-1 monoclonal antibody (2 μg mL^{-1}), rabbit-Rab7 monoclonal antibody (2 μg mL^{-1}), or rabbit LAMP-1 (1 μg mL^{-1}) for 1.5 h, followed by washing three times with PBS and further incubation for 1 h with dual-labeled AF555/AF647 goat anti-rabbit conjugate secondary antibody (2 μg mL^{-1}).

STORM imaging was performed using the same parameters as described above. Lasers (488, 561, and 647 nm) were used for excitation of the fluorophores. For each channel, 5,000–10,000 frames were acquired. STORM images were processed, and the population of nano-objects was analyzed using the STORM module of the NIS Elements Nikon software. A list of localizations by Gaussian fitting the fluorescence spots of blinking dyes were processed by the software, which also allowed for drift correction. Blinking events that are detected in consecutive frames are counted as single molecules by the software. For each sample, 10–12 cells were analyzed with approximately 200 nano-objects per cell to obtain colocalization statistics.

Cytokine Secretion: RAW 264.7 cells were plated in 96-well plates at a density of 1×10^4 cells per well overnight. Then, cells were incubated with the TA–ODN NPs (containing 100 nM CpG) in fresh medium. Cells were incubated at 37 °C for 24 h and the supernatant was collected for

TNF-α analysis (ELISA), using protocols recommended by the manufacturer. As a control experiment, the release of cytokines from cells stimulated by TA–ODN NPs prepared with no CpG was also measured. For the time-course experiment, cells were treated with TA–ODN NPs (CpG:100 nM) at 37 °C for 2, 4, 8, and 24 h, and the supernatants were collected and stored at − 80 °C prior to ELISA.

RESULTS AND DISCUSSION

Preparation and Characterization of TA–ODN NPs

Controlling the morphology, size, and composition of NPs obtained by the supramolecular co-assembly of biomolecules, while avoiding the formation of large and polydisperse aggregates, can be challenging. The three-dimensional arrangement of the interacting biomolecules, as well as the morphology and composition of the obtained complex, depends on the concentrations of the building blocks, the nature and strength of the interactions involved in the complexation, and the kinetics of the assembly process. TA is a water-soluble polyphenol that exists in the aggregated form in aqueous solution above its critical micelle concentration ($5–10$ g L^{-1})[25] in a pH range of 3–7.5. Self-aggregation of TA in aqueous solution was indicated by hydrodynamic diameter measurements of 300–400 nm, which are higher than the expected size of single small TA molecules.[26] Intermolecular hydrophobic interactions between the aromatic rings are considered key to stabilizing TA into high molecular weight clusters or polydisperse nanoaggregates in aqueous solution. Therefore, we first examined the presence of intermolecular TA clusters in aqueous solution (5 mg mL^{-1}) by nuclear magnetic resonance (NMR) spectroscopy and high-performance liquid chromatography (HPLC). The ^{1}H NMR spectrum of TA solution acquired at 25 °C showed broad signals in the range of 6.5–7.5 ppm, which were attributed to the aromatic

protons of the galloyl groups, indicating that TA was in the aggregated state (Figure S1a). The sharp peak at 7.2 ppm was attributed to gallic acid molecules that are typically present in commercial TA samples. After subjecting the TA solution to a heat treatment at 80 °C for 1 h, an increase of an order of magnitude in signals attributed to TA was observed (Figure S1a). This observation indicates that heating causes breakage of the hydrogen bonds and $\pi-\pi$ stacking interactions among the TA molecules, resulting in smaller and more mobile aggregates and individual TA molecules. When the TA solution was cooled to 25 °C, the intensity of the NMR signals in the range of 6.5–7.5 ppm decreased, indicating that the TA molecules re-assembled into larger aggregates (Figure S1a). The extent of hydrolysis of TA into gallic acid was small during thermal treatment, as indicated by the small increase in the peak area (~25 %) of gallic acid at 3.7 min in the HPLC chromatogram of the treated TA solution relative to that of the untreated sample (Figure S1b,c).

The synthesis of TA–ODN NPs was first attempted by mixing TA with a single-stranded (ss) ODN at room temperature (20 °C). However, incomplete complexation of the ODN molecules and formation of micrometer-sized aggregates (Figure S2) were observed. These results were attributed to the rapid and uncontrolled aggregation of ODNs with the TA aggregates. Hence, we hypothesize that heating the mixture of TA and ODN to 80–90 °C for 1 h and slowly cooling (~0.5 °C s^{-1}) to room temperature (23°C) would first induce the disassembly of TA nano-aggregates and then enable the controlled arrangement of TA and ODN molecules into uniform NPs, as stabilized by both hydrogen bonding and $\pi-\pi$ stacking interactions, as depicted in **Scheme 1**.
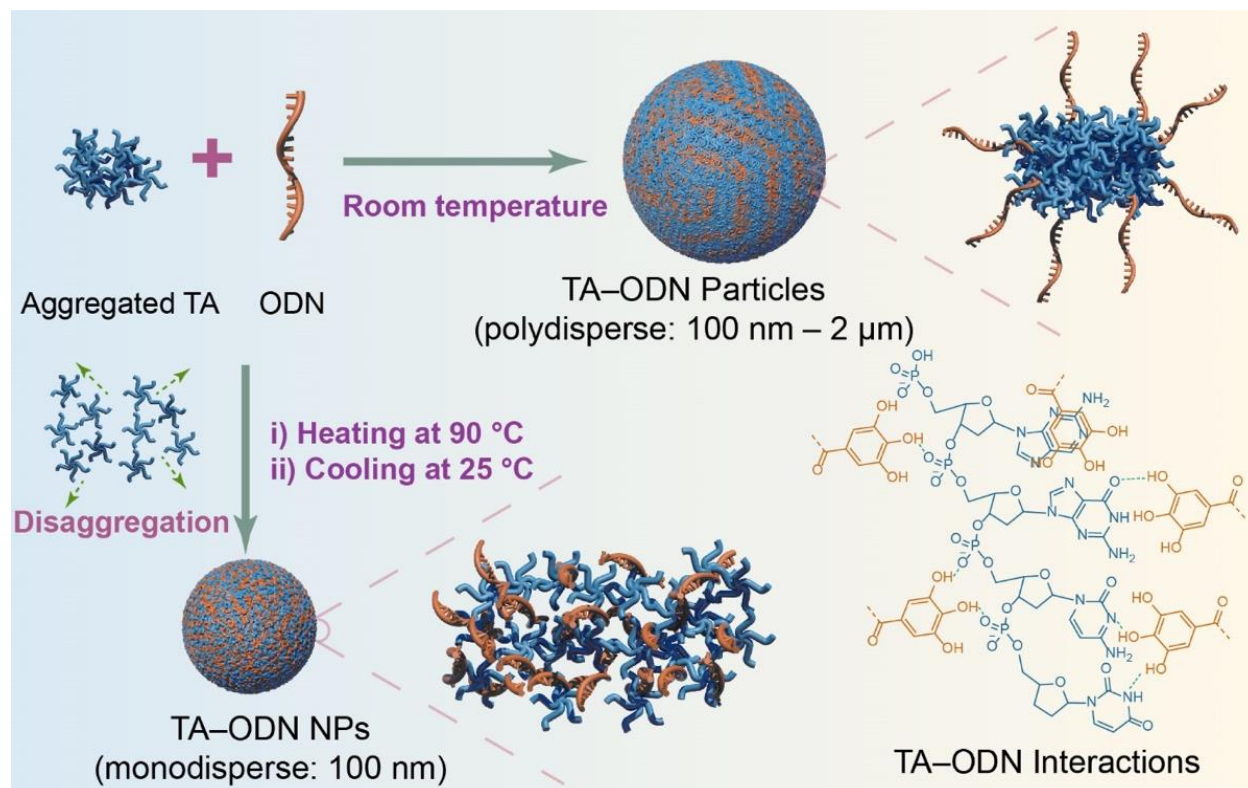
Scheme 1. Schematic of the supramolecular assembly of TA and ssDNA. At room temperature, large polydisperse aggregates are formed, whereas monodisperse nanoparticles are formed upon thermal cycling (heating–cooling) treatment; these monodisperse NPs are stabilized by hydrogen bonding and π–π stacking interactions.

To verify our hypothesis and directly probe the complexation of TA and DNA into TA–ODN NPs, super-resolution microscopy (STORM) was used. This imaging technique enabled the visualization of individual TA–ODN NPs with nanoscale resolution based on the detection of single-molecule localizations (**Figure 1**). As super-resolution imaging allowed both the size and composition of the TA–ODN NPs to be simultaneously determined, individual TA–ODN NPs could be resolved after formation at equilibrium conditions.[27] TA–ODN NPs were prepared by mixing TA and ODNs at varying TA/ODN weight ratios (w/w) from 1 to 12, where the

concentration of ODN was fixed (38 μM). To obtain an optimal signal density for STORM imaging, only one-fourth of the required DNA strands were used in the labeled form for the preparation of TA–ODN NPs. The product of complexation was deposited on a glass coverslip for TIRF-STORM imaging (Figure 1a). A clustering analysis script was used to quantify the size of the TA–ODN NPs and the number of single ODN molecules inside individual NPs. Of note, each DNA molecule carries a photoswitchable fluorophore Alexa Fluor 647 (AF647). Hence, the experimentally detected localizations are proportional to the number of DNA molecules assembled into the TA–ODN NPs.
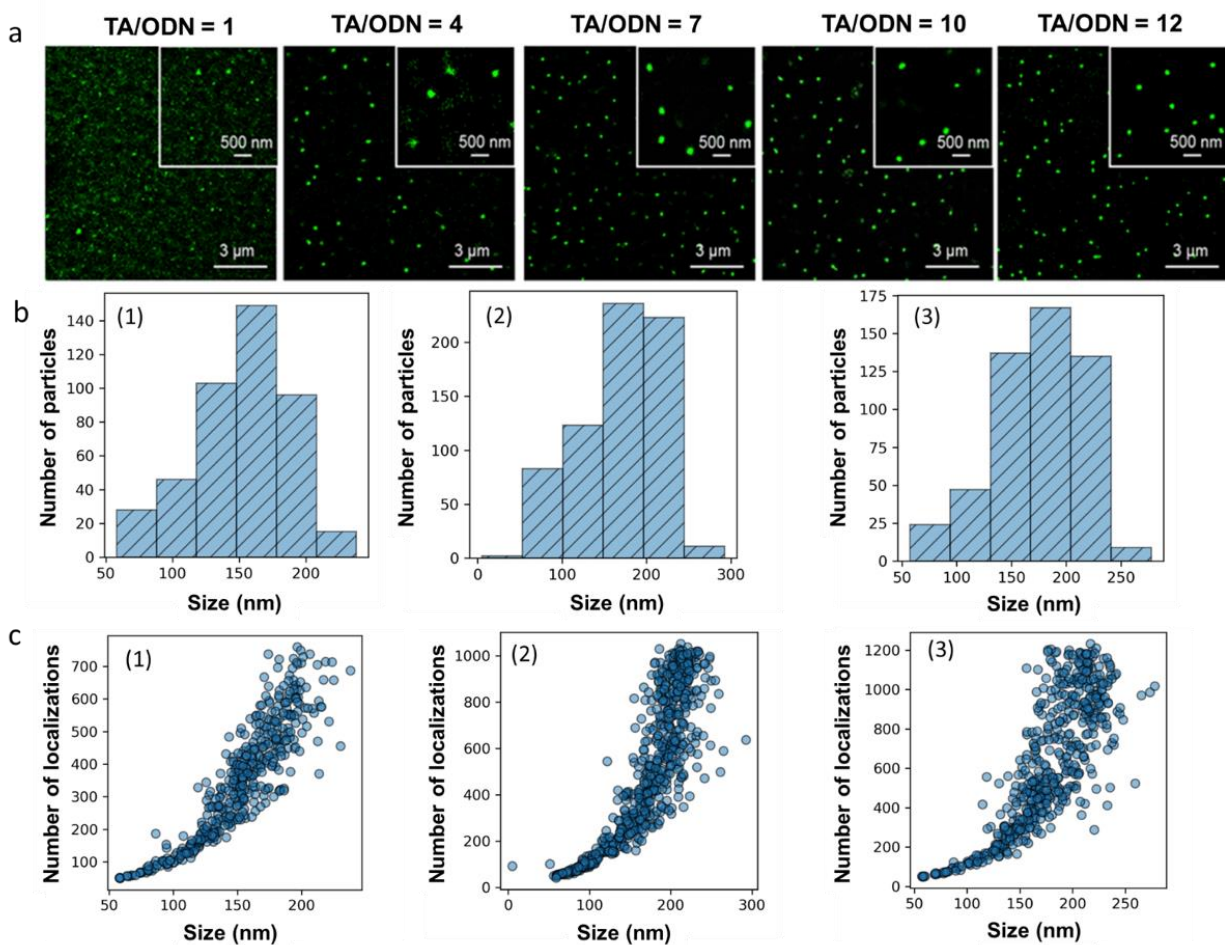
Figure 1. Complexation of TA and ODNs at the molecular level. (a) STORM images of TA–ODN NPs (green signal) prepared at TA/ODN ratios of 1, 4, 7, 10, and 12. (b) Frequency histograms of the diameter of TA–ODN NPs determined by STORM imaging and (c) scatter plots of number of localizations (N) as a function of diameter of TA–ODN NPs; the TA–ODN NPs were prepared at TA/ODN ratios of (1) 7, (2) 10, and (3) 12.

As seen in Figure 1a, at TA/ODN ratios of 1 and 4, a large amount of signal on the glass coverslip was observed, which corresponds to free DNA molecules not associated with the TA–ODN NPs. However, upon increasing the TA/ODN ratio from 7 to 12, the presence of free ODN molecules became negligible, indicating that more nucleic acid molecules were incorporated in the TA–ODN NPs. Moreover, uniform, and spherical NPs were observed at TA/ODN ratios of 7–12. The frequency histograms shown in Figure 1b compare the sizes of the TA–ODN NPs prepared at different TA/ODN ratios, as imaged by STORM. The diameters of the NPs increased from 151 ± 36 nm to 168 ± 46 and 174 ± 40 nm as the TA/ODN ratio increased from 7 to 10 and 12, respectively (Figure 2b).

Figure 1c shows scatter plots of the number of localizations, N, as a function of the diameters of the imaged TA–ODN NPs (Figure 2c). The number of localizations, which is proportional to the number of ODN molecules, increased with an increase in the diameter and therefore the volume of the TA–ODN NPs. The TA–ODN NPs prepared at TA/ODN ratios of 10 and 12 showed an overall higher number of DNA molecules (1000–1200 localizations at 250 nm) incorporated in a single nanoparticle compared to the TA–ODN NPs prepared at a TA/ODN ratio of 7 (maximum 700 localizations). It is worth noting that, as only one-fourth of the assembled ODN molecules are fluorescently labeled, the effective number of ODN molecules packed in the TA–ODN NPs is fourfold. To quantitatively correlate the localization and molecule counts, each ODN molecule,

14

which is considered to bear one AF647 probe, can blink several times during acquisition, typically 1–3 times in our experimental setup. By estimating the statistical distribution of the blinking events in a single ODN molecule under the same experimental conditions, the localization counts can be correlated with the number of ODN strands. However, this photophysical phenomenon depends on the local environment of fluorophores, which is likely different in the assembled and non-assembled states. Therefore, it is difficult to strictly determine the exact number of ODN molecules embedded into the TA–ODN NPs from the number of localizations.

For the subsequent studies, TA–ODN NPs prepared at a TA/ODN ratio of 10 were selected because of their optimal diameter (~170 nm) for cellular studies, and efficient and homogeneous packing of DNA molecules (**Figure 2**a). The TA–ODN NPs had a ζ-potential of -18 ± 1 mV, as measured by microelectrophoresis.

Of note, TA–ODN NPs maintained their colloidal stability and size during storage at 4 °C up to one month observation (Figure S3).

The stability of TA–ODN NPs in solutions containing 10% and 100 % fetal bovine serum (FBS), was investigated by STORM imaging studies. Notably, in the presence of serum proteins remained well dispersed (Figure S4a) and intact. A comparison of size distributions obtained by processing the STORM images revealed that the size of the TA–ODN NPs increased from 168 ± 46 nm (Figure 1b2) to 218 ± 50 and 280 ± 60 nm (Figure S4b) after incubation with 10 and 100 % FBS respectively. In addition, the ζ-potential of the TA–ODN NPs changed from -18 ± 1 to -27 ± 4 mV after incubation with 100 % FBS. Overall, these results indicate that the adsorption of serum proteins on TA–ODN NPs causes a moderate broadening of size distribution without compromising the colloidal stability of nanoparticles.

Furthermore, scanning electron microscopy (SEM) (Figure 2b), transmission electron microscopy (TEM) (Figure 2c), and atomic force microscopy (AFM) (Figure 2d,e) all showed well-dispersed TA–ODN NPs of approximately 100 nm in size in air-dried conditions. The TA–ODN NPs in the dry state showed a thickness of ~16 nm (Figure 2e), as measured from AFM. Overall, the electron and atomic microscopy images indicate that the TA–ODN NPs are highly hydrated and undergo shrinkage upon drying. To give an insight into the effect of ODN sequences length on the supramolecular assembly process, we prepared TA–ODN NPs using ODN with different lengths (15mer, 47mer and 60mer) and compared the particles size distributions (Figure S5). We successfully obtained TA–ODN NPs with single stranded ODN molecules ranging from 15 to 60 bases, however an increase in particle size and broadening of distribution as a function of ODN length was observed. In summary, we have shown that thermal cycling of TA/ODNs mixture is a simple and effective strategy to control the supramolecular assembly of polyphenols and single stranded nucleic acids with different molecular weights with high ODN loading capacity and tunable size.
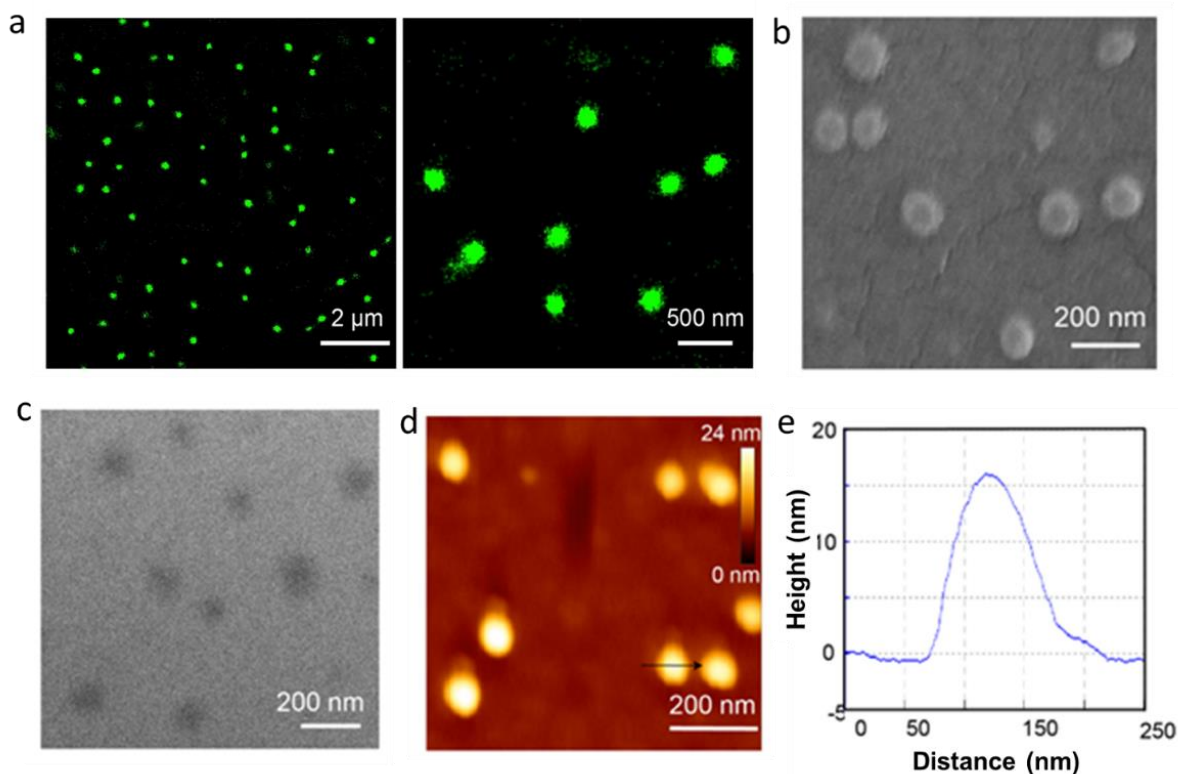
Figure 2. (a–e) Characterization of TA–ODN NPs (prepared at TA/ODN ratio of 10) in the hydrated state by super-resolution microscopy, STORM (a), and dry state by SEM (b), TEM (c), and AFM (d and e).

Intracellular Trafficking and Bioactivity of TA–ODN NPs

To evaluate the intracellular bioactivity of the TA–ODN NPs, AF647-labeled ssDNA containing CpG sequences was used for NP synthesis. In response to intracellular CpG delivery, immune cells, such as macrophages, secrete several cytokines, including tumor necrosis factor (TNF)-α. These cytokines subsequently amplify the immune responses to vaccines and immunotherapies.[28] CpG sequences are recognized by Toll-like receptor 9 (TLR9), which is expressed in the endosomes of immune cells. However, naked ODN-bearing CpG moieties are not stable in serum owing to their susceptibility to deoxyribonuclease (DNase) and are difficult to transport through

cell membranes because of their negative charge. Hence, the intracellular delivery of functional CpG would benefit from the encapsulation and delivery by NPs, as the carrier not only protect the cargo molecules from the extracellular and intracellular enzymatic degradation but also enable highly efficient cellular internalization by endocytosis and controlled and sustained release of CpG moieties in the endosomes.

The cytotoxicity of the TA–ODN NPs (at varying DNA concentrations) was measured after incubation with RAW 264.7 cells for 24 h at 37 °C. As observed in **Figure 3**a, the TA–ODN NPs showed negligible cytotoxicity against RAW 264.7 cells. The percentage of AF647-labeled TA–ODN NP-associated cells reached 40% after 2 h and 90% after 24 h incubation (Figure 3b, Figure S6). To investigate the cellular internalization of the TA–ODN NPs, RAW 264.7 cells were incubated with AF647-labeled TA–ODN NPs for 2, 4, 8, and 24 h. A strong fluorescence signal was observed in the cells, indicating that the NPs were efficiently taken up by RAW264.7 cells (Figure 3c, Figure S7).
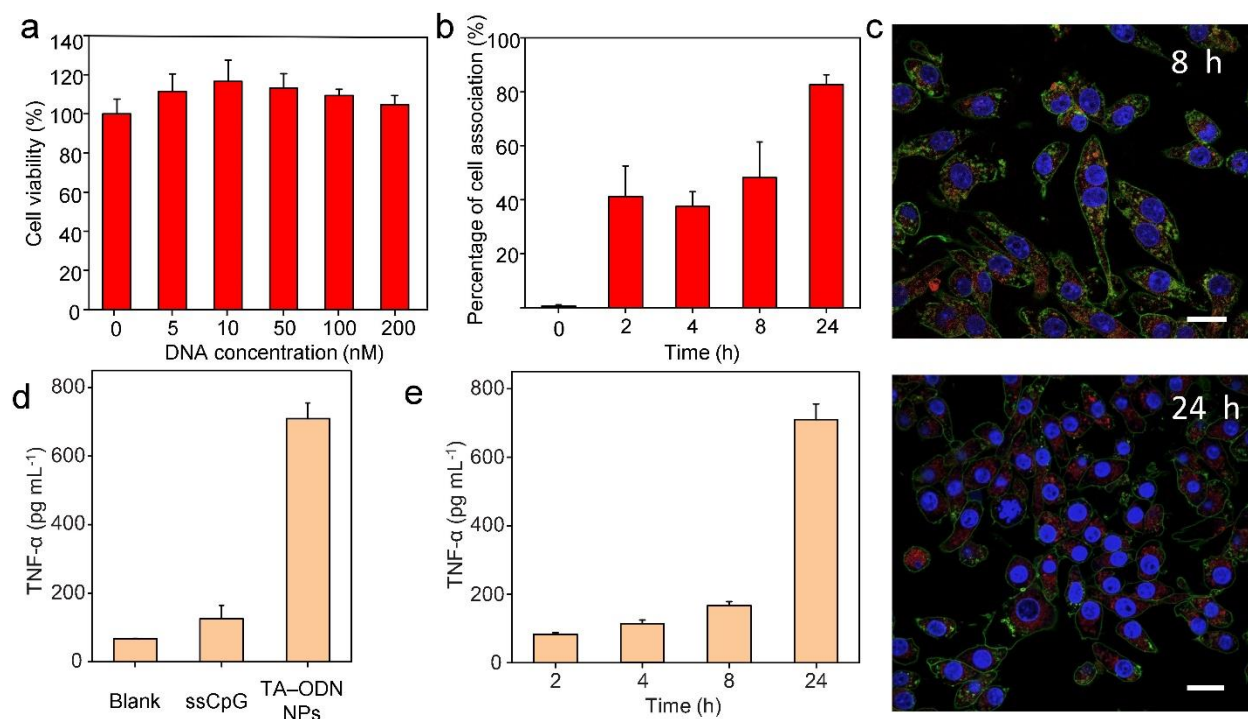
Figure 3. Interactions of TA–ODN NPs (containing CpG) with immune cells. (a) MTT assay of viability of RAW 264.7 cells after incubation for 24 h with TA–ODN NPs at different TA–ODN NPs concentrations (corresponding to DNA concentrations). (b) Cell association kinetics of TA–ODN NPs after incubation for 2, 4, 8, and 24 h, as investigated by flow cytometry. (c) Representative confocal laser scanning microscopy images of cells after incubation with TA–ODN NPs (DNA 100 nM) for 8 and 24 h; scale bars: 10 μm. Cell membranes are stained with AF488–WGA (green), nuclei are stained with Hoechst (blue), and TA–ODN NPs are labeled with AF647 (red). (d) Secretion levels of TNF-α from untreated cells (blank) and cells stimulated by ssCpG or TA–ODN NPs for 24 h (CpG: 100 nM). (e) Secretion of TNF-α from cells incubated with TA–ODN NPs (CpG: 100 nM) for 2, 4, 8, and 24 h. Data are shown as mean ± standard deviation (SD) (n = 3).

The potential of the TA–ODN NPs to trigger cytokine secretion was investigated. TA–ODN NPs (CpG concentration: 100 nM) were incubated with RAW 264.7 cells at 37 °C for 24 h. As observed from Figure 3d, a significantly higher level (up to 7-fold) of TNF-α was observed in RAW 264.7 cells when incubated with the TA–ODN NPs than with free CpG. The cytokine production induced by the TA–ODN NPs was time-dependent (Figure 3e). Cytokine production was limited and increased slightly as the incubation times increased from 2 to 8 h. In contrast, a significant increase in TNF-α secretion was observed upon incubation for 24 h. These results are consistent with the slow association process observed in Figure 4b. In addition, the compact structure of the TA–ODN NPs may protect the ODN strands from degradation by DNase inside the endosomal compartments and consequently delay the exposure of CpG to the TLR9 receptor. Collectively, these results show that CpG-containing TA–ODN NPs can efficiently activate macrophages to secrete cytokines, however the molecular mechanism of activation remains elusive.

Multicolor STORM was used to gain a deeper insight in the mode of trafficking and intracellular localization of the TA–ODN NPs. Cells were exposed to dual-labeled TA–ODN NPs (AF488/AF647-Green) for 4 h. The culture medium was then replaced, and the incubation continued for 0, 4, and 24 h. The cells were fixed after 0, 4, and 24 h incubation. The early endosomes, late endosomes, and lysosome vesicles were labeled for early endosome antigen 1, Rab 7, and lysosomal-associated membrane protein 1, respectively, and subsequently with the dual-labeled secondary antibody AF555/AF647-Red. Representative STORM images acquired after incubation of RAW 264.7 cells with the TA–ODN NPs are shown in **Figure 4**a and Figure S6. The TA–ODN NPs imaged inside the cells were categorized as either colocalized (with early endosomes, late endosomes, and lysosomes) or noncolocalized (Figure 4b). To quantify the extent of colocalization of the TA–ODN NPs with the endo-lysosomal compartments, statistical analysis

of the acquired STORM images as a function of incubation time was performed (Figure 4c). At each time point, $n = 10$–12 cells and $n = 200$ nano-objects/cells were analyzed. These data suggest that most TA–ODN NPs are confined within the endo-lysosomal compartments in the first 8 h of incubation with cells. However, a longer incubation time of 28 h significantly reduced the extent of colocalization of TA–ODN NPs with all vesicles. Specifically, the lack of colocalization of the TA–ODN NPs with the compartments at 28 h suggests that endosomal escape of the assembled TA–ODN NPs occurs. STORM imaging revealed that most of the ODN molecules localized in the cytosol remained assembled into nanostructures even after incubation for 48 h (Figure S8a). Nevertheless, the widespread signal of single DNA molecules in the cell cytoplasm indicates the disassembly of the TA–ODN NPs disassembly or degradation of DNA by intracellular DNase (Figure S7b). We hypothesize that the slow translocation of intact TA–ODN NPs to the cytosol is likely mediated by the limited pH buffering capacity of TA (pK_a ~6) in the pH range of 5.6–6.7 and the proton sponge effect mechanism.[29] Overall, these results indicate that the endocytic trafficking of TA–ODN NPs to the cytosol occurs through early, late endosomes, and lysosomes within 28 h at 37 °C. When confined in the endosomes, the TA–ODN NPs can effectively expose the CpG motif from the three-dimensional nanostructure to engage TLR9 receptors and trigger signaling pathways.
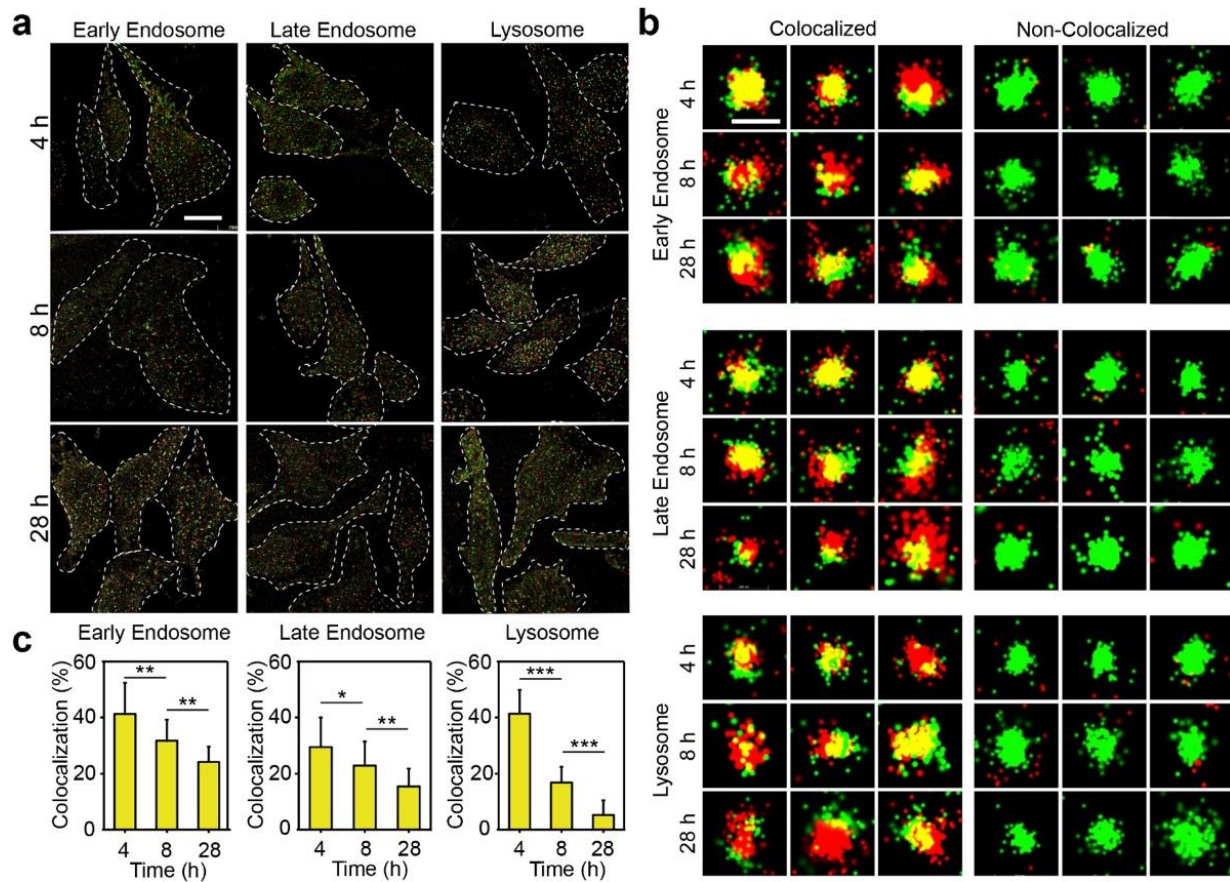
Figure 4. Intracellular trafficking and disassembly of TA–ODN NPs in RAW 264.7 cells by super-resolution microscopy. (a) Representative multicolor STORM images of RAW 264.7 cells incubated for 4, 8, and 28h with TA–ODN NPs (green signal) and stained for early endosomes, late endosomes, and lysosomes (red signal, scale bar= 6μm. (b) Representative high-magnification images of the intracellular TA–ODN NPs and vesicles (image size = 200 nm). The red signal represents the intracellular vesicles, and the green signal represents the TA–ODN NPs. RAW 264.7 cells were treated with TA–ODN NPs at different incubation times (4–48 h). (c) Statistical analysis of TA–ODN NPs colocalized and noncolocalized with early endosomes, late endosomes, and lysosomes as a function of incubation time. Data are shown as mean ± SD ($n = 3$). For each time point, $n =10–12$ cells and $n = 200$ nano-objects/cell were analyzed. The significantly different

22

values ($p < 0.05$) between the bars are denoted by *. Statistical significance was determined using one-way analysis of variance with a 95% confidence interval and Tukey's multiple comparisons.

CONCLUSION

We developed a simple, one-pot, template-, metal-, and polymer-free supramolecular assembly process in aqueous solution to organize ODN and TA molecules into stable and functional NPs. We showed that thermal cycling is key to controlling the supramolecular arrangements of TA and ODN molecules. The efficiency of complexation of the TA and ODN molecules and the architecture of the obtained NPs were assessed at the molecular level using single-molecule super-resolution microscopy. TA–ODN NPs bearing CpG sequences were effectively internalized by macrophages and escaped from endo/lysosomes and promoted a higher level of cytokine production compared to free CpG. Super-resolution microscopy also revealed the endosomal escape of the TA–ODN NPs and subsequent release of ODN in the cytosol. Overall, the engineered NPs have potential for the intracellular delivery of nucleic acids, including gapmer antisense ODNs, aptamers, and splice switching ODNs, to cytoplasmic or nuclear targets with the ultimate aim to develop systems to treat cancer, infections, and autoimmune diseases.

ASSOCIATED CONTENT

Supporting Information. ^{1}H NMR spectra of TA aqueous solution (5 mg mL^{-1}) recorded at 25 °C (red), after heating at 80 °C for 1 h (green), and subsequent cooling to 25 °C (blue); HPLC chromatogram of commercial TA showing the presence of different polyphenol species, including gallic acid (3.7 min) and TA (10–30 min); HPLC chromatogram of TA after heating at 80 °C for 1

h; Size distribution of TA–ODN NPs obtained at room temperature (red curve) and after heating and cooling (black curve), as determined by dynamic light scattering; STORM image showing the stability of TA–ODN NPs (prepared at TA/ODN ratio of 10) after incubating with cell culture medium containing 10% FBS for 24 h; Mean fluorescence intensity (MFI) of cells treated with AF647-labeled TA–ODN NPs at varying incubation times of 0, 2, 4, 8, and 24 h at 37 °C, as measured by flow cytometry; Representative confocal laser scanning microscopy images showing the cellular uptake of TA–ODN NPs as a function of incubation time at 37 °C; Representative multicolor STORM images of the RAW 264.7 cells exposed for 4, 8, and 28 h to TA–ODN NPs; Representative multicolor STORM images of RAW 264.7 cells exposed for 48 h to TA–ODN NPs.

AUTHOR INFORMATION

#YQ and HZ contributed equally to this work

Corresponding Author

* fcaruso@unimelb.edu.au

* francesca.cavalieri@rmit.edu.au

Author Contributions

The manuscript was written through contributions of all authors. All authors have given approval to the final version of the manuscript.

Notes

The authors declare no competing financial interest.

REFERENCES

(1)   Tan, X.; Jia, F.; Wang, P.; Zhang, K. Nucleic acid-based drug delivery strategies. *J. Control. Release* **2020**, *323*, 240-252.

(2)   Li, M.; Wang, C.; Di, Z.; Li, H.; Zhang, J.; Xue, W.; Zhao, M.; Zhang, K.; Zhao, Y.; Li, L. Engineering Multifunctional DNA Hybrid Nanospheres through Coordination-Driven Self-Assembly. *Angew. Chem. Int. Ed. Engl.* **2019**, *58*, 1350-1354.

(3)   Kroll, A. V.; Jiang, Y.; Zhou, J.; Holay, M.; Fang, R. H.; Zhang, L. Biomimetic Nanoparticle Vaccines for Cancer Therapy. *Adv. Biosyst.* **2019**, 3, e1800219.

(4)   Riley, M. K.; Vermerris, W. Recent Advances in Nanomaterials for Gene Delivery—A Review**.** *Nanomaterials* **2017**, *7*, 94.

(5)   Huang, P.; Wang, X.; Liang, X.; Yang, J.; Zhang, C.; Kong, D.; Wang, W. Nano-, micro-, and macroscale drug delivery systems for cancer immunotherapy. *Acta Biomater.* **2019**, *85*, 1-26.

(6)   Ho W.; Gao M.; Li F.; Li Z.; Zhang X-Q; Xu X. Next-Generation Vaccines: Nanoparticle-Mediated DNA and mRNA Delivery. *Adv. Health. Mat.* **2021**, *10*, 2001812.

(7) Luther, D.C.; Huang R.; Jeon, T.; Zhang X.; Lee Y.W.; H. Nagaraj H.; Rotello V.M., Delivery of drugs, proteins, and nucleic acids using inorganic nanoparticles. *Adv. Drug Deliv. Rev.* **2020**, 156, 188–213.

(8)   Lai, W. F.; Wong, W. T. Design of Polymeric Gene Carriers for Effective Intracellular Delivery. *Trends Biotechnol.* **2018**, *36*, 713-728.

(9)   Kim, H. J.; Kim, A.; Miyata, K.; Kataoka, K. Recent progress in development of siRNA delivery vehicles for cancer therapy. *Adv. Drug Deliv. Rev.* **2016**, *104*, 61-77.

(10)   Lu R.; Zhang X.; Cheng X.; Zhang Y.; Zan X. Zhang L. Medical Applications Based on Supramolecular Self-Assembled Materials From Tannic Acid. *Front. Chem.* **2020**, *8*, 583484.

(11)   Zhou, J.; Lin, Z.; Ju, Y.; Rahim, M. A.; Richardson, J. J.; Caruso, F. Polyphenol-Mediated Assembly for Particle Engineering. *Acc. Chem. Res.* **2020**, *53*, 1269-1278.

(12)   Wu, S.; Yan, Y.; Ni, D.; Pan, X.; Chen, X.; Guan, J.; Xiong, X.; Liu, L. Development of a safe and efficient gene delivery system based on a biodegradable tannic acid backbone. *Colloids Surf. B: Biointerfaces* **2019**, *183*, 110408.

(13)   Li, N.; Yang, X.; Liu, W.; Xi, G.; Wang, M.; Liang, B.; Ma, Z.; Feng, Y.; Chen, H.; Shi, C. Tannic Acid Cross-linked Polysaccharide-Based Multifunctional Hemostatic Microparticles for the Regulation of Rapid Wound Healing. *Macromol. Biosci.* **2018**, *18*, e1800209.

(14)   Shin, M.; Ryu, J. H.; Park, J. P.; Kim, K.; Yang, J. W.; Lee, H. DNA/Tannic Acid Hybrid Gel Exhibiting Biodegradability, Extensibility, Tissue Adhesiveness, and Hemostatic Ability. *Adv. Funct. Mater.* **2015**, *25*, 1270-1278.

(15)   Fan, H.; Wang, L.; Feng, X.; Bu, Y.; Wu, D.; Jin, Z. Supramolecular Hydrogel Formation Based on Tannic Acid. *Macromolecules* **2017**, *50*, 666-676.

(16)   Wang, X.; Yan, J.; Wang, L.; Pan, D.; Xu, Y.; Wang, F.; Sheng, J.; Li, X.; Yang, M. Oral delivery of anti-TNF antibody shielded by natural polyphenol-mediated supramolecular assembly for inflammatory bowel disease therapy. *Theranostics* **2020**, *10*, 10808-10822.

(17)   Le, Z.; Chen, Y.; Han, H.; Tian, H.; Zhao, P.; Yang, C.; He, Z.; Liu, L.; Leong, K. W.; Mao, H.-Q.; Liu, Z.; Chen, Y. Hydrogen-Bonded Tannic Acid-Based Anticancer Nanoparticle for Enhancement of Oral Chemotherapy. *ACS Appl. Mater. Interfaces* **2018**, *10*, 42186-42197.

(18)   Le, Z.; Liu, Z.; Sun, L.; Liu, L.; Chen, Y. Augmenting Therapeutic Potential of Polyphenols by Hydrogen-Bonding Complexation for the Treatment of Acute Lung Inflammation. *ACS Appl. Bio Mater.* **2020**, *3*, 5202-5212.

(19)   Chen, J.; Pan, S.; Zhou, J.; Lin, Z.; Qu, Y.; Glab, A.; Han, Y.; Richardson, J. J.; Caruso, F. Assembly of Bioactive Nanoparticles via Metal–Phenolic Complexation. *Adv. Mater.* **2022**, *34*, 2108624.

(20)   Han, Y.; Lin, Z.; Zhou, J.; Yun, G.; Guo, R.; Richardson, J. J.; Caruso, F. Polyphenol-Mediated Assembly of Proteins for Engineering Functional Materials. *Angew. Chem. Int. Ed. Engl.* **2020**, *59*, 15618-15625.

(21)   Qu Y.; De Rose R.; Kim C-J; Zhou J.; Lin Z.; Ju Y.; Bhangu S.K.; Cortez-Jugo C.; Cavalieri F.; Caruso F. Supramolecular Polyphenol-DNA Microparticles for In Vivo Adjuvant and Antigen Co-Delivery and Immune Stimulation. *Angew. Chem. Int. Ed. Engl.* **2023**, *62*, e202214935.

(22)   Chen B-M; Cheng T-Lu; Roffler S.R. Polyethylene Glycol Immunogenicity: Theoretical, Clinical, and Practical Aspects of Anti-Polyethylene Glycol Antibodies. *ACS Nano* **2021**, *15*, 14022-14048.

(23)   Hoang Thi, T. T.; Pilkington, E. H.; Nguyen, D. H.; Lee, J. S.; Park, K. D.; Truong, N. P. The Importance of Poly(ethylene glycol) Alternatives for Overcoming PEG Immunogenicity in Drug Delivery and Bioconjugation. *Polymers* **2020**, *12*, 298.

(24)   Ha J.; Cui Y.; Gu Z.; Yang D. Controllable assembly/disassembly of polyphenol-DNA nanocomplex for cascade-responsive drug release in cancer cells. *Biomaterials* **2021**, 273, 120846.

(25)   Cala O.; Dufourc E.J.; Fouquet E.; Manigand C.; Laguerre M.; Pinaet I. The Colloidal State of Tannins Impacts the Nature of Their Interaction with Proteins: The Case of Salivary Proline-Rich Protein/Procyanidins Binding. *Langmuir* **2012**, 28, 17410-17418.

(26)   Dultz S.; Mikutta R.; Kara SNM; Woche S.K.; Guggenberger G. Effects of solution chemistry on conformation of self-aggregated tannic acid revealed by laser light scattering. *Sci. Total Environ.* **2021**, *754*, 142119.

(27)   Feiner-Gracia N.; Olea R. A.; Fitzner R.; El Boujnouni N.; van Asbeck A.H.; Brock R.; Albertazzi L. Super-resolution Imaging of Structure, Molecular Composition, and Stability of Single Oligonucleotide Polyplexes. *Nano Letters* **2019**, *19*, 2784-2792.

(28)   Iwasaki A.; Medzhitov R. Toll-like receptor control of the adaptive immune responses. *Nat. Immunol.* **2004**, *5*, 987-995.

(29)   Degors I. M. S.; Wang C.; Rehman Z.U.; Zuhorn I. S. Carriers Break Barriers in Drug Delivery: Endocytosis and Endosomal Escape of Gene Delivery Vectors. *Acc. Chem. Res.* **2019**, *52*, 1750-1760.

Table of Contents graphic